Electrically Programmable On-Chip Equivalent-Phase-Shifted Waveguide Bragg Grating on Silicon

Weifeng Zhang, *Member, IEEE*, and Jianping Yao, *Fellow, IEEE, Fellow, OSA*

(Top-Scored Paper)

***Abstract*—We report an electrically programmable equivalent-phase-shifted (EPS) waveguide Bragg grating implemented on silicon with programmable spectral response. Equivalent phase shift through nonuniform sampling in a Bragg grating is an effective solution to realize a phase-shifted Bragg grating, which significantly reduces the requirement for fabrication accuracy by three orders of magnitude as compared with the fabrication of a conventional phase-shifted Bragg grating. In this paper, an EPS Bragg grating with an equivalent phase shift introduced by increasing one sampling period in the grating center by a half sampling period is proposed, and the tuning of the phase shift is enabled by incorporating two independent PN junctions in each sampling period. Through controlling the bias voltages applied to the PN junctions, the spectral response of the EPS Bragg grating is tuned. The proposed EPS waveguide grating is fabricated and its performance is experimentally evaluated. A multichannel EPS Bragg grating with programmable spectral response is demonstrated. The key advantages of implementing EPS Bragg gratings include largely reduced fabrication constraint and strong multichannel tuning capability, which opens new avenues for on-chip Bragg gratings for programmable multichannel signal processing.**

***Index Terms*—Equivalent phase-shifted (EPS) grating, free-carrier plasma dispersion effect, sampled waveguide grating, silicon photonics, waveguide Bragg grating.**

I. Introduction

SINCE the discovery of fiber Bragg gratings (FBGs) by Hill and co-workers in 1978 [1], FBGs have played a key role in the fields of telecommunications and optical sensing [2]–[4]. With the rapid development of photonic integrated circuit (PICs), on-chip waveguide Bragg gratings have been extensively researched [5]–[8]. In particular, thanks to the compatibility with the mature CMOS process and potential for seamless integration with electronics, great efforts have been directed to the study of using silicon as a photonic integration material system [9]. Recently, silicon-based integrated Bragg gratings with different index modulation profiles have been demonstrated [10]–[12]. By using different tuning mechanisms, tunable silicon-based Bragg gratings have also been reported [13]–[17]. By integrating other photonic elements on a same chip, an on-chip grating-based signal processor can be realized for multifunctional signal processing [18]–[23]. However, there is a long-standing limitation in a conventional Bragg grating - the grating spectral response is predetermined by its index modulation profile, which is fixed once the grating is fabricated. To date, most of the gratings, either fiber- or waveguide-based, are fabricated with a specific index modulation profile for a user-defined task. Although different mechanisms have been employed to tune the spectral response, these tuning approaches are mainly limited to the shift of the center wavelength. For many applications, however, the tuning of the other spectral characteristics, such as the spectral shape and the phase response, should be implementable. For example, a grating with a tunable bandwidth is useful in reconfigurable wireless communications systems [24]. To perform tunable fractional order temporal differentiation and Hilbert transformation [25], a grating with a tunable phase jump at the center frequency is needed.

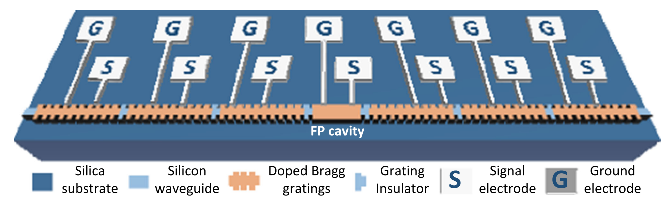

Fig. 1. Schematic view of a reconfigurable waveguide Bragg grating.

To meet such requirement, recently we have proposed a fully reconfigurable waveguide Bragg grating and experimentally demonstrated such a grating on a silicon photonic chip [26], [27]. Fig. 1 shows the perspective view of the fully reconfigurable grating. It consists of multiple series-connected uniform Bragg grating sections and a Fabry-Perot (FP) cavity section in the center. Each uniform Bragg grating section is made by creating periodic corrugations on the waveguide sidewalls, and an independent lateral PN junction is incorporated in the waveguide.

Manuscript received July 7, 2018; revised November 4, 2018 and December 5, 2018; accepted December 19, 2018. Date of publication January 1, 2019; date of current version February 20, 2019. This work was supported in part by the Natural Science and Engineering Research Council of Canada (NSERC) through the CREATE program and the CMC Microsystems, and in part by the NSERC under the Silicon Electronic-Photonic Integrated Circuits CREATE program. *(Corresponding author: Jianping Yao.)*

The authors are with the Microwave Photonics Research Laboratory, School of Electrical Engineering and Computer Science, University of Ottawa, Ottawa, ON K1N 6N5, Canada (e-mail: wzhan088@uottawa.ca; jpyao@eecs.uottawa.ca).

Color versions of one or more of the figures in this paper are available online at http://ieeexplore.ieee.org.

Digital Object Identifier 10.1109/JLT.2018.2889414

To achieve electrical insulation, an un-doped grating is used between two adjacent sections to function as an insulator. Distributed electrodes are connected to the PN junctions. By applying a bias voltage to a PN junction, the refractive index of the grating in that particular section could be tuned locally based on free-carrier plasma dispersion (FCPD) effect. By incorporating multiple PN junctions, the entire index modulation profile of the grating could be electrically reconfigured by field programming all the bias voltages, which enables the grating to have diverse spectral characteristics for diverse applications.

The concept was verified by a proof-of-concept demonstration in which a reconfigurable grating with two identical uniform sub-grating sections and a FP cavity section in the middle was fabricated. Thanks to the independently controllable PN junctions, the fabricated grating could be reconfigured to be a uniform, a phase-shifted, and a chirped grating by programming the bias voltages. By incorporating the fabricated grating in a microwave photonic system, a programmable microwave signal processor with three signal processing functions including temporal differentiation, true time delay, and microwave frequency identification was implemented [27]. Compared to a micro-ring resonator-based photonic signal processor [28], the reconfigurable waveguide grating has a higher fabrication tolerance. In addition, the design and implementation of a complicated directional coupler, which is required in a micro-ring resonator, is avoided.

The key to implement the reconfigurable grating [26], [27] is to introduce an accurate phase shift, which is usually in the order of one quarter of the Bragg wavelength, and thus a stringent fabrication accuracy is required to make an accurate phase shift. The major limitation in implementing a phase-shifted Bragg grating on silicon is the poor spectral accuracy due to the poor fabrication tolerance. To have a precise spectral response, high-precision lithography must be used, but it is not available at this time. To implement a Bragg grating having a precise spectral response without using high-precision lithography, a solution is to use the equivalent-phase-shifted (EPS) grating technique [29]. An equivalent phase shift can be achieved based on nonuniform spatial sampling of a uniform Bragg grating. By controlling the sampling profile, a high-precision EPS Bragg grating with different spectral response can be achieved [30], [31]. Since the sampling period is in micrometer range while the grating pitch is in nanometer range, a requirement for fabrication accuracy is reduced by three orders of magnitude as compared with the conventional fabrication technique. Recently, an EPS waveguide grating on silicon was demonstrated [32], [33]. Since the sampling profile was fixed, the spectral response was fixed and could not be tunable.

In this paper, we report a programmable EPS waveguide Bragg grating implemented on silicon. In the EPS waveguide Bragg grating, an equivalent π phase shift is introduced to a Bragg grating by increasing one sampling period in the center by a half sampling period. The tuning of the phase shift is enabled by incorporating two independent PN junctions in each sampling period, with one in the on-modulation grating section and the other in the off-grating section. By controlling the bias voltages applied to the PN junctions, the equivalent phase shift can be tuned, which leads to a programmable on-chip EPS Bragg grating. The proposed EPS Bragg grating device is fabricated and its performance is experimentally evaluated. Thanks to the spatial sampling, an EPS Bragg grating with a multi-channel spectral response is demonstrated. By programming the bias voltages, the equivalent phase shifts can be tuned, making the spectral response programmable. In the demonstration, an EPS Bragg grating with a tunable resonant wavelength and tunable extinction ratio without changing the resonance wavelength is achieved. The key advantages of the implementation of the proposed ESP Bragg grating include a largely reduced fabrication constraint and a strong multichannel tuning capability, which opens new avenues for on-chip gratings to achieve multichannel signal processing.

II. Chip Design and Fabrication

Fig. 2(a) illustrates the schematic of a programmable EPS waveguide Bragg grating on a silicon photonic chip. The inset gives the zoom-in view of the grating, which is produced by creating the periodic corrugations on the waveguide sidewall. Three TE-mode grating couplers are used to couple light into and out of the chip. A light wave generated by a laser diode (LD) is coupled into the device via an input grating coupler and sent to the EPS Bragg grating. If the wavelength of the light wave satisfies the Bragg condition, the light wave would be reflected. A Y-branch coupler is used to collect the reflected light wave, which is sent to a reflection grating coupler for out-of-chip coupling. Note that another half of the reflected light wave is directed to the input grating coupler, potentially disturbing the laser source. To minimize the effect of unwanted reflection, it is necessary to incorporate an optical isolator at the input port of the Y-branch coupler, especially when heterogeneous integration is employed where an III–V laser source is incorporated on a silicon platform [35]. Other wavelengths will transmit through the grating and be coupled out of the chip via a transmission grating coupler. To minimize the chip size and reduce the bending loss, a wire waveguide is mostly used to guide the light wave in the chip. Fig. 2(b) shows a zoom-in view of the EPS Bragg grating. An equivalent phase shift is realized by spatially sampling a uniform grating to create an increased sampling period $P + \Delta\mathrm{L}$ in the center for the grating, where *P* is spatial sampling period and $\Delta\mathrm{L}$ is the sampling period increment. If a uniform grating with a grating pitch Λ is spatially sampled with a spatial sampling function having a sampling period *P,* where $P \gg \Lambda$, a multiple channel transmission spectrum will be produced [30]. The 0-th channel is centered at the Bragg wavelength $\lambda_{\mathrm{B}} = 2n_{eff}\Lambda$ and the channel spacing *CS* is given by

$$CS = \frac{2n_{eff}\Lambda^2}{P} \tag{1}$$

where n_{eff} is the effective refractive index of the grating waveguide.

The increased sampling period $P + \Delta\mathrm{L}$ in the center would introduce an equivalent phase shift in the odd-order channels.

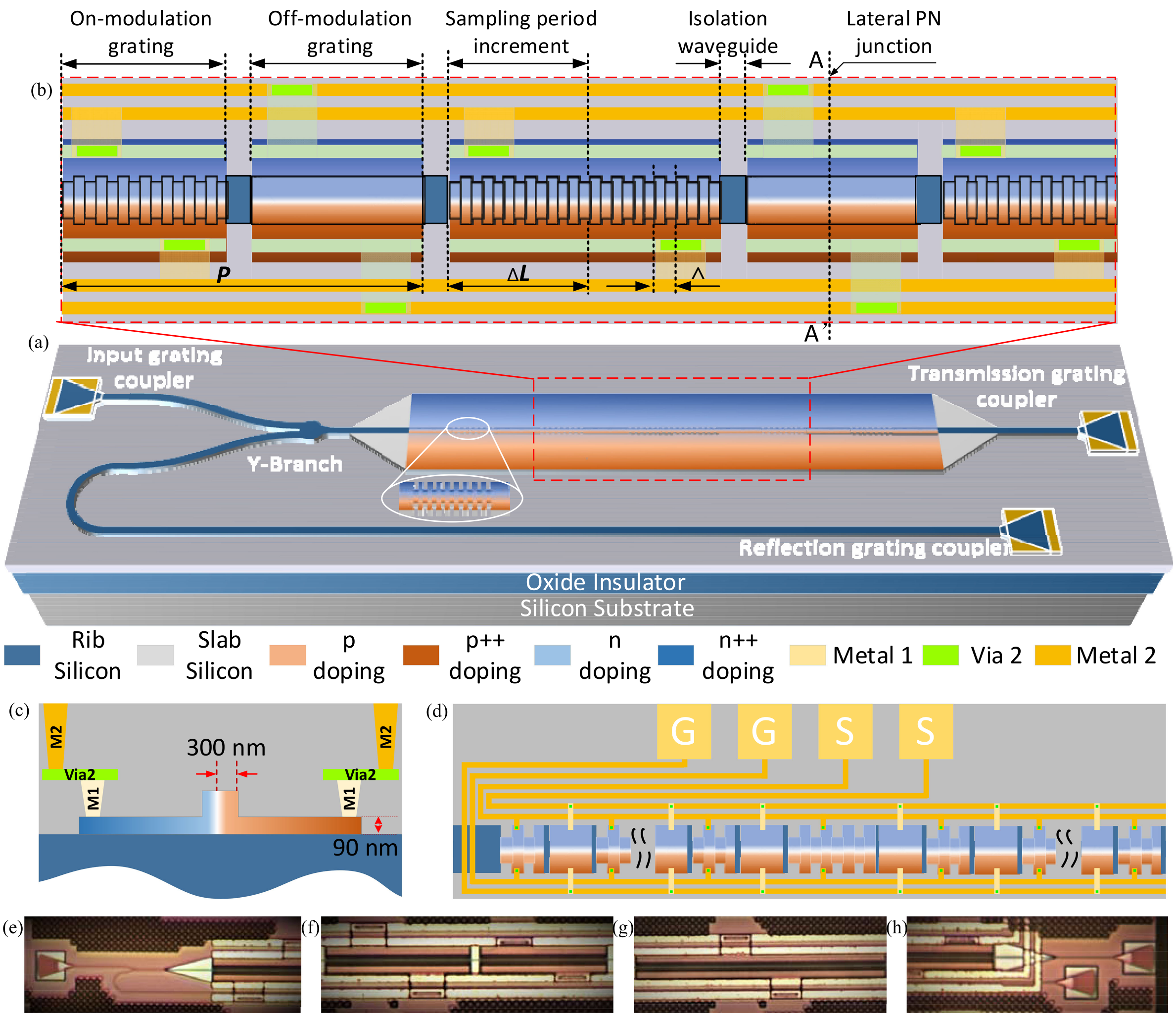

Fig. 2. (a) Perspective view of the proposed programmable EPS waveguide Bragg grating on a silicon photonic chip; (b) zoom-in view of the grating structure; (c) cross-sectional view of the waveguide with doping in the grating; (d) top-view of the designed EPS Bragg grating, (e) photograph of the input grating coupler, (f) photograph of a sampling period in the fabricated grating, (g) photograph of the increased sampling period ΔL, and (h) photograph of transmission and reflection grating couplers.

The equivalent phase shift is given by [34]

$$\Delta\varphi = n\frac{2\pi}{P}\Delta L \tag{2}$$

where n is the channel order.

In the design, the sampling period increment is selected to be $\Delta \mathrm{L} = P/2$, which leads to an odd integer number of π phase shift to the odd-order channels. In the implementation of a conventional phase-shifted grating, a phase shift block with a length of $\Lambda/2$ is added in the center to generate a quarter-wave phase shift. Considering the sampling period P is three orders of magnitude larger than the grating pitch Λ, the requirement for lithography accuracy would be highly reduced. In addition, by manipulating the sampling period P, a new degree of freedom in the grating design is enabled, which offers the flexibility in producing a grating with arbitrary spectral response. For example, by linearly increasing the sampling period, an equivalent-chirped grating could be realized [36].

To make the grating electrically programmable, independent lateral PN junctions are incorporated along the grating. As shown in Fig. 2(b), in a sampling period, two independent PN junctions are distributed in the on-modulation grating section and off-modulation grating section. To avoid mutual electrical coupling between neighboring PN junctions, a section of undoped waveguide is used as an electrical insulator. Fig. 2(c) shows the cross-sectional view of the lateral PN junction along the dashed line AA' in Fig. 2(b). To support a single fundamental TE mode operation, a silicon rib waveguide with 500-nm in width, 220-nm in height, and 90-nm in slab thickness is employed. To achieve high-speed tuning, a lateral PN junction is produced in the rib waveguide. Since the FCPD effect is more sensitive to the change of the free-hole concentration, to achieve a higher tuning efficiency, an asymmetrical lateral PN junction is used by slightly shifting the junction center of 50 nm to the left from the waveguide center. Thus, the optical mode overlap with the p-type doping region is increased. Additional p++ and n++ implantations, 1 μm away from the rib to minimize absorption losses, are utilized for ohmic contact formation.

Fig. 2(d) gives the top-view of the proposed EPS Bragg grating. In our design, the entire device has 11 sampling periods in total. In the whole EPS Bragg grating, all the PN junctions in the on-modulation grating sections are connected and share one pair of the electrical contacts, and all the off-modulation grating sections are connected and share another pair of the electrical contacts. Thus, by controlling the bias voltages for the on-modulation grating sections and the off-modulation grating sections, based on FCPD effect in silicon, the grating pitch Λ, the sampling length P and the sampling period increment could be tuned, which provides full reconfigurability of the EPS Bragg grating. The key advantages of the programmable ESP Bragg grating include largely reduced requirements for fabrication accuracy and significantly increased tuning capability.

The programmable EPS Bragg grating is fabricated at IME in a CMOS-compatible process using 193-nm deep ultraviolet lithography. The grating is fabricated on a silicon-on-insulator (SOI) substrate with a bottom silica layer of 2 μm in thickness and a top silicon layer of 220 nm in thickness. Fig. 2(e) is a photograph of the input grating coupler of the fabricated grating captured by a microscope camera. A double-layer linear taper waveguide with a length of 50 μm is used for mode transition between the wire and the rib waveguides. Fig. 2(f) gives a photograph of one sampling period of the EPS Bragg grating. The grating pitch Λ is 310 nm with a duty cycle of 50%, and the periodic sidewall corrugation has a depth as large as 100 nm, which makes the grating work in the C band. The spatial sampling period P is 255.75 μm including a 7.75-μm-long undoped waveguide for electrical insulation. Fig. 2(g) provides a photograph of the increased sampling period in the center of the EPS Bragg grating. The sampling period increment ΔLis chosen to be 124 μm for an odd integer number of π phase shift in the odd-order channels. Fig. 2(h) gives a photograph of the transmission and reflection grating couplers. Again, a double-layer linear taper waveguide with a length of 50 μm is used for the mode transition between the wire and the rib waveguides. The entire device has a length of 3.2 mm and a width of 0.25 mm in total, giving a small footprint of 0.8 mm^2.

Compared with a conventional phase-shifted Bragg grating, the EPS Bragg grating is markedly advantageous in terms of implementation flexibility, repeatability, and cost-effectiveness, which are highly suitable for mass production. These features become more important when multiple and variable phase shifts are needed. In addition, the availability of phase shift tuning via electrically tuning the distributed PN junctions gives a new degree of freedom in the spectrum tuning, which is useful for programmable signal processing.

III. Chip Performance Evaluation

An optical vector analyzer (LUNA OVA CTe) is used to measure the reflection and transmission spectra of the fabricated EPS Bragg grating, and two high-precision source meters (Keithley 2400) are used to provide the bias voltages. During the performance evaluation, a thermoelectric-cooler (TEC) is used to control and stabilize the chip temperature. The silicon photonic chip is placed on top of the TEC, and a thermistor is placed adjacent to the chip, to measure and provide a feedback temperature to a commercial TEC controller. During the experiment, the chip temperature is stabilized at 23 °C, the temperature of the room where the experiment is performed.

A. Reflection and Transmission Spectra

Fig. 3(a) shows the measured reflection and transmission spectra of the fabricated EPS Bragg grating in the static state. The red line shows the measured transmission spectrum, while the blue line shows the measured reflection spectrum. Thanks to the spatial sampling, the grating has a multichannel reflection and transmission spectra. Due to the equivalent phase shift caused by the increased sampling period, in the odd-order channels, a passband in the transmission stopband and a notch in the reflection passband are observed, which are the typical spectral features of a phase-shifted Bragg grating and confirms the effectiveness of the EPS approach in the implementation of a phase-shifted Bragg grating. In addition, in the reflection spectrum of the 0-th order channel, several notches are observed, which are resulted from the strong index modulation of the silicon waveguide grating. The insertion loss of the EPS Bragg grating is 26 dB, which includes the fiber-to-fiber I/O coupling loss of 15 dB and the grating loss of 11 dB. By optimizing the grating coupler design and enhancing the etching uniformity with the use of more advanced lithography process, the I/O coupling loss and the grating sidewall scattering loss could be significantly reduced. Fig. 3(b) shows the reflection and transmission spectra of the negative-order channels. As can be seen, only the odd-order channels have EPS-resulted spectral features, while the even-order channels have spectral responses that are not affected by the EPS. This is understandable because all even-order channels would have a phase shift that is an integer number of 2π. The channel spacing is extracted to be 1.2 nm, and the theoretical value given by (1) is 1.1 nm, a good match is resulted. Thanks to the strong index modulation of the waveguide grating, the 11th channel spectral response could still be seen. In addition, compared with the strong spectral responses of the odd-order channels, the even-order channels have much weaker spectral responses. This is because the even-order modes are easily coupled into the cladding, which undermines the grating effect. In addition, when the order number is increasing, the spectral response becomes weaker due to the reduction in the grating effect. Fig. 3(c) shows the reflection and transmission spectra of the positive order channels. The spectral responses of the odd-order channels with EPS-resulted spectral features are clearly seen, while the spectral responses of the even-order channels disappear, which, again, is due to the coupling of the even-order modes into the cladding.

As a distinct feature of an EPS Bragg grating is that multichannel phase shifts could be introduced, which offers the possibility for simultaneous manipulation of multiple wavelengths, thus increasing the capability of the grating for programmable multichannel signal processing. For example, an EPS Bragg grating with well controlled channel spacing can be employed in a WDM system for advanced multichannel signal processing [37], [38].

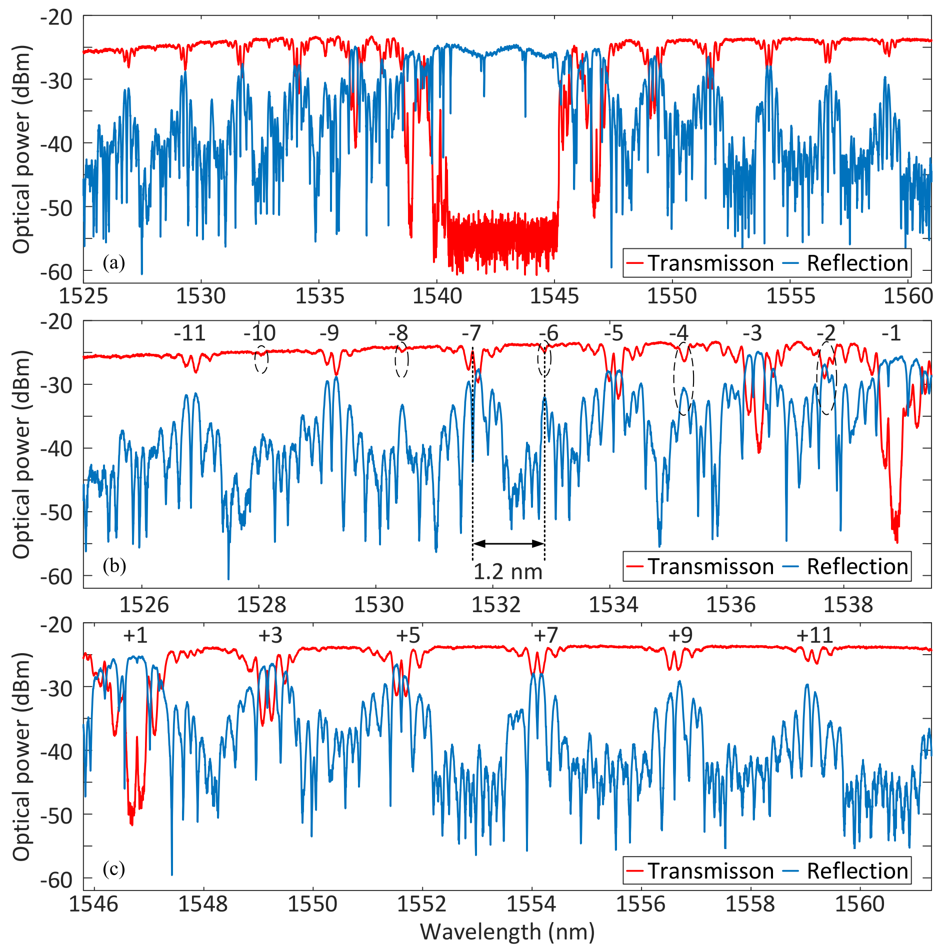

Fig. 3. (a) Measured reflection and transmission spectra of the fabricated EPS Bragg grating, (b) zoom-in view of the reflection and transmission spectra of the negative-order channels; and (c) zoom-in view of the reflection and transmission spectra of the positive-order channels.

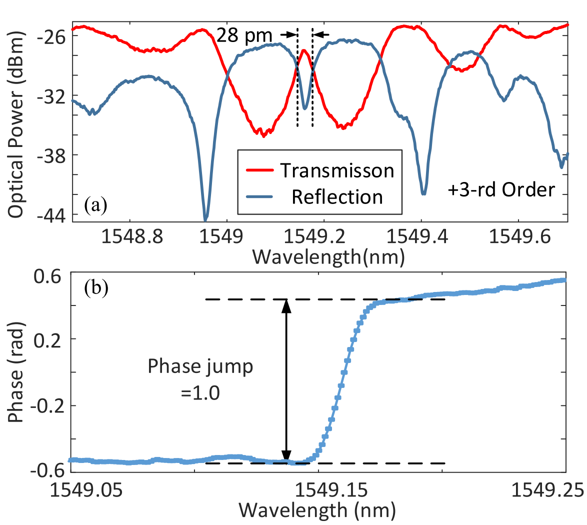

Fig. 4. (a) Measured reflection and transmission spectra of the +3rd channel and (b) the phase response of the reflection notch in the reflection spectrum.

B. Tuning of the EPS Bragg Grating

Since the PN junctions in the on-modulation grating sections are connected and the PN junctions in the off-modulation grating sections are connected, too, one DC voltage is needed to bias the PN junctions in the on-modulation grating sections and a second DC voltage is needed for the off-modulation grating sections. To clearly illustrate the spectral tuning, a zoom-in view of the +3rd channel spectral response is presented. Fig. 4(a) shows the measured reflection and transmission spectra of the +3rd channel in the static state. It can be seen that a passband is produced in the stopband in the transmission spectrum and a notch is produced in the passband of the reflection spectrum. The notch in the reflection band has a 3-dB bandwidth of 28 pm. The Q-factor is calculated to be 55,300 and the extinction ratio is 6.4 dB. Fig. 4(b) shows the phase response of the reflection notch. At the notch center, there is a phase jump of 1.0, which is smaller than the expected value of π. The difference is resulted due to the ion implantations. The extinction ratio could be increased by changing the grating index modulation and sampling period.

First, a bias voltage is applied to the PN junctions in the on-modulation grating sections, while the PN junctions in the off-modulation grating sections are kept in the static state. Fig. 5(a) shows the measured resonant wavelength shift when the bias voltage varies from -19 to $+1$ V. For a PN junction being reverse biased, more carriers are extracted from the junction and thus the depletion region is widened. Based on the

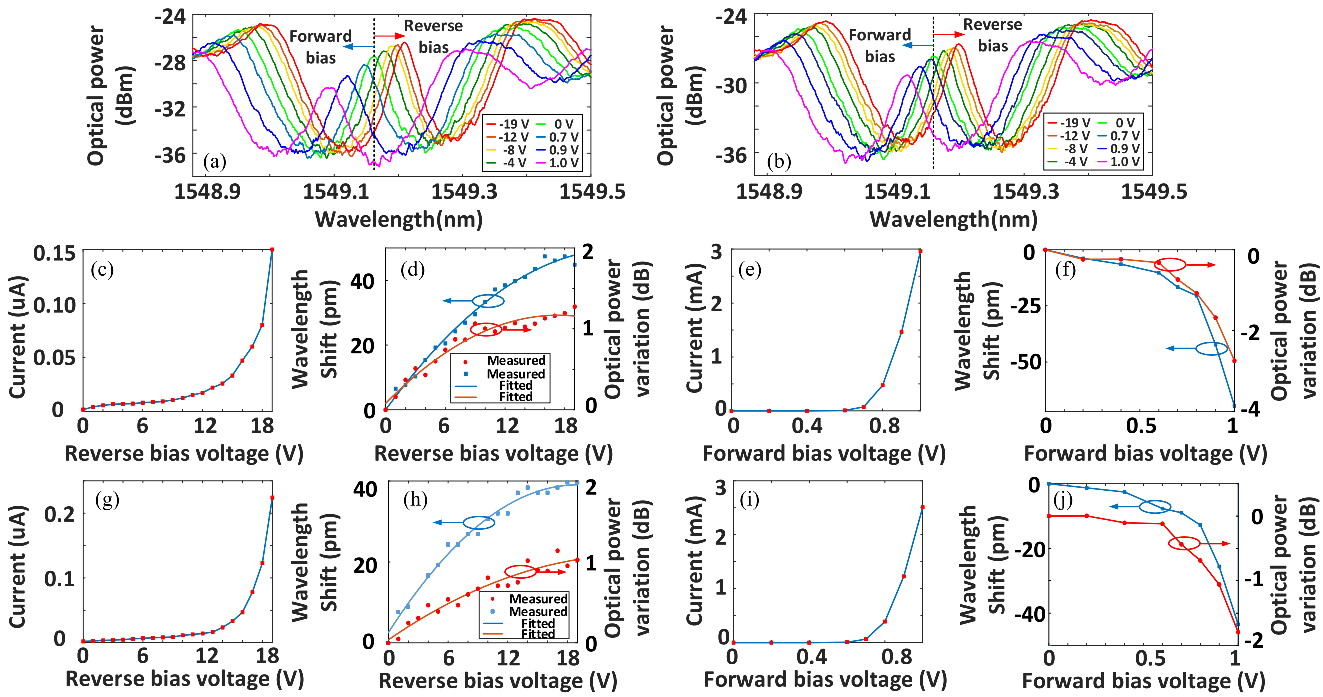

Fig. 5. Measured transmission spectra of the +3rd channel when the two bias voltages are separately applied. (a) Measured transmission spectra of the +3rd channel when the bias voltage applied to the on-modulation grating sections is sweeping; (b) measured transmission spectrum of the +3rd channel when the bias voltage applied to the off-modulation grating sections is sweeping; (c) V-I curve when the PN junctions in the on-modulation grating sections are reverse biased; (d) transmission window peak wavelength shift and peak power variation when the PN junctions in the on-modulation grating sections are reverse biased; (e) V-I curve when the on-modulation grating sections are forward biased; (f) transmission window peak wavelength shifting and peak power variation when the PN junctions in the on-modulation grating sections are forward biased; (g) V-I curve when the PN junctions in the off-modulation grating sections are forward biased; (h) transmission window peak wavelength shift and peak power variation when the PN junctions in the off-modulation grating sections are reverse biased; (i) V-I curve when the PN junctions in the off-modulation grating sections are forward biased; (j) transmission window peak wavelength shift and peak power variation when the PN junctions in the off-modulation grating sections are forward biased.

FCPD effect, the effective refractive index would be increased, which would lead to a red-shifted spectrum. For a PN junction being forward biased, a large amount of free carriers are injected into the waveguide, which would lead to a decreased effective refractive index and thus a blue-shifted spectrum. Then, the bias voltage is applied to the PN junction in the off-modulation grating sections, while the PN junctions in the on-modulation grating sections are kept in the static state. Fig. 5(b) shows the measured resonant wavelength shift when the bias voltage varies from −19 to +1 V. A red shift in resonant wavelength happens when a reverse bias voltage is applied, and a blue shift happens when a forward bias voltage is applied.

Fig. 5(c) shows the voltage–current (V-I) curve of the PN junctions in the on-modulation grating sections for the PN junctions being reverse biased. The PN junctions reaches breakdown at a voltage of approximately −18 V. Fig. 5(d) shows the transmission window peak wavelength shift and peak power variation when the PN junctions in the on-modulation grating sections are reverse biased. As can be seen, the peak wavelength in the resonant window is red shifted and the peak power is increased, which is due to the reduced optical absorption induced by the free carriers. At a maximum applied bias voltage of −19 V in the measurement, a maximum peak wavelength shift of 49 pm is achieved with a power consumption of 2.85 μW. Fig. 5(e) shows the V-I curve of the PN junctions in the on-modulation grating sections for the PN junctions being forward biased, which indicates that the PN junctions are turned on at a voltage of about +0.7 V. Fig. 5(f) shows the peak wavelength shift in the transmission window and peak power variation when the PN junctions in the on-modulation grating sections are forward biased. As can be seen, the peak wavelength in the transmission window is blue shifted and the peak power is decreased, which is due to the increased optical absorption induced by the injected free carriers. At a maximum forward bias voltage of +1.0 V in the measurement, the notch wavelength has a shift of 70 pm with a power consumption of 2.90 mW.

Fig. 5(g) shows the V-I curve of the PN junctions in the off-modulation grating sections for the PN junctions being reverse biased. The PN junctions reach breakdown at approximately −18 V. Fig. 5(h) shows the peak wavelength shift in the transmission window and peak power variation when the PN junctions in the on-modulation grating sections are reverse biased. As can be seen, the peak wavelength in the resonant window is red shifted and the peak power is increased, which is again due to the reduced absorption caused by the extraction of the injected free carriers. At a maximum applied bias voltage of −19 V in the measurement, a maximum peak wavelength shift of 40 pm is achieved with a power consumption of 4.26 μW. Fig. 5(i) shows the V-I curve of the PN junctions in the off-modulation grating sections for the PN being forward biased, which indicates that the PN junctions are turned on at a voltage of about +0.7 V. Fig. 5(j) shows the transmission window wave-

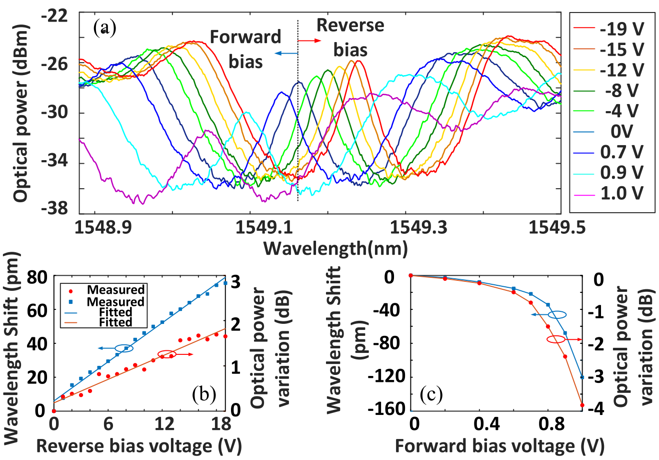

Fig. 6. (a) Measured transmission spectrum of the +3rd channel when two bias voltages are synchronously sweeping; (b) transmission window peak wavelength shifting and its power variation when the PN junctions are reverse biased; and (c) transmission window peak wavelength shifting and its power variation when the PN junctions are forward biased.

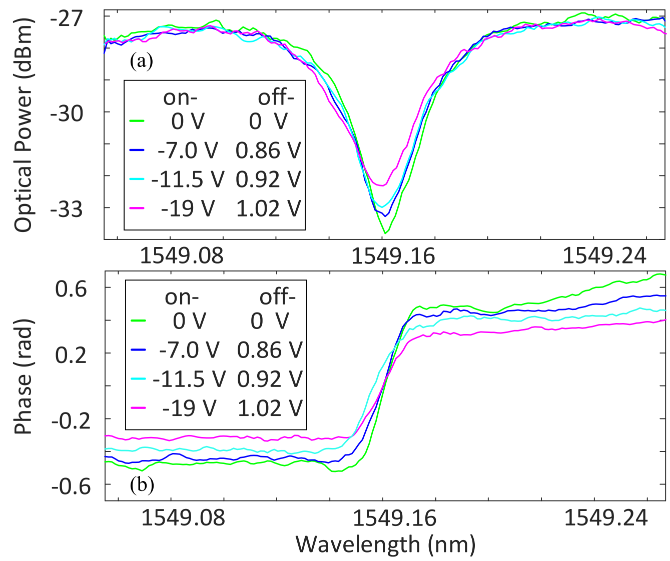

Fig. 7. (a) Tuning of the extinction ratio of the reflection notch in the +3rd channel with the notch wavelength kept unchanged, and (b) tuning of the phase jump of the reflection notch in the +3rd channel.

length shift and peak power variation when the PN junctions in the on-modulation grating sections are forward biased. As can be seen, the peak wavelength in the transmission window is blue shifted and the peak power is decreased, which is due to the increased optical absorption induced by the injection of free carriers. At a maximum forward bias voltage of +1.0 V in the measurement, the peak wavelength has a shift of 43 pm with a power consumption of 2.52 mW.

The measurement results show that by applying and tuning a bias voltage to the PN junctions in the on-modulation or the off-modulation grating sections, the refractive index change in that specific section would lead to an independent tuning of the spectral response of the grating. Thus, by field programming the bias voltages, the grating could be electronically reconfigured.

C. Programming the EPS Bragg Grating

When the two bias voltages are simultaneously and synchronously changed from −19 to +1 V, the grating spectrum would be shifted. Fig. 6(a) shows the measured reflection and transmission spectra of the grating. For the PN junctions being reverse biased, the spectrum is red shifted; while, for the PN junctions being forward biased, the spectrum is blue shifted. Fig. 6(b) shows the peak wavelength in the transmission window shift and peak power variation. As can be seen, the transmission window peak wavelength is red shifted and the peak power is increased, which is due to the reduced absorption caused by the extracted free carriers. At a maximum applied bias voltage of −19 V in the measurement, a maximum peak wavelength shift of 78 pm is achieved with a power consumption of 2.83 μW. Fig. 6(c) shows the peak wavelength shift in the transmission window and peak power variation. As can be seen, the transmission window peak wavelength is blue shifted and the peak power is decreased, which is due to the increased optical absorption induced by the injected free carriers. At the maximum forward bias voltage of +1.0 V in the measurement, the notch wavelength has a shift of 120 pm with a power consumption of 2.46 mW.

Since the PN junctions in the on-modulation and off-modulation grating sections can be independently controlled, the spectrum shift induced by each junction could cancel each other. Thus, the resonant wavelength can be maintained unchanged, while the extinction ratio and phase jump of the reflection notch can be changed. Fig. 7(a) shows the tuning of the extinction ratio while the notch wavelength is maintained unchanged for different bias voltage combinations. It is known that in a conventional phase-shifted Bragg grating, it is not possible to tune the extinction ratio while maintaining the notch wavelength unchanged. In the fabricated grating, by field programming the bias voltages, the notch wavelength shifts induced by the on- and off-modulation grating sections can counteract. Thus, the notch wavelength can be kept unchanged, while different bias voltage combinations could lead to a different loss, which leads to a different extinction ratio. As shown in Fig. 7(a), the extinction ratio is changed from 6.4 to 4.5 dB. Fig. 7(b) shows the phase response of the reflection notch in the +3rd channel. As can be seen, by programming the bias voltages, the phase jump at the notch center can be tuned from 1.0 to 0.48. The tuning range could be increased by controlling all the PN junctions in the grating.

IV. Discussion and Conclusion

As demonstrated, an EPS Bragg grating implemented on silicon could be made programmable by changing the bias voltages to the PN junctions. For the fabricated EPS Bragg grating, we have demonstrated that the resonant wavelength and the extinction ratio could be tuned. Extinction ratio tuning without changing the wavelength is a unique feature of this EPS Bragg grating, an important feature for signal processing.

In conclusion, we have proposed and experimentally demonstrated an electrically programmable EPS waveguide Bragg grating implemented on silicon. An equivalent phase shift was introduced via nonuniform spatial sampling. Since the requirement for fabrication accuracy for spatial sampling is 3 orders of magnitude less than that by using conventional phase shift approach, the requirement for lithography accuracy was significantly reduced. In our demonstration, an EPS Bragg grating with 11 sampling periods was fabricated, in which one equivalent phase shift was introduced by increasing sampling period in the center by half spatial sampling period, and the tuning of the phase shift was enabled by incorporating two independent PN junctions in the on- and off-modulation grating sections. A multichannel EPS Bragg grating was experimentally demonstrated. By programming the bias voltages, the resonant wavelength could be shifted and the extinction ratio could be tuned while maintaining the resonance wavelength unchanged. The key advantages of the proposed EPS Bragg grating solution include a largely reduced fabrication constraint, and a significantly increased multi-channel tuning capability, which opens new avenues for on-chip gratings for multichannel signal processing.

Acknowledgment

We acknowledge CMC Microsystems, for providing the design tools and enabling the fabrication of the device.

References

[1] K. O. Hill, Y. Fujii, D. C. Johnson, and B. S. Kawasaki, “Photosensitivity in optical fiber waveguides: Application to reflection filter fabrication,” *Appl. Phys. Lett.*, vol. 32, pp. 647–649, Aug. 1978.

[2] A. Othenos and K. Kalli, *Fiber Bragg Gratings: Fundamentals and Applications in Telecommunications and Sensing*. Norwood, MA, USA: Artech House, 1999.

[3] T. L. Yeo, Tong Sun, K. T. V. Grattan, D. Parry, R. Lade, and B. D. Powell, “Polymer-coated fiber Bragg grating for relative humidity sensing,” *IEEE Sensors J.*, vol. 5, no. 5, pp. 1082–1089, Oct. 2005.

[4] Z. Wei, H. M. H. Shalaby, and H. Ghafouri-Shiraz, “Modified quadratic congruence codes for fiber Bragg-grating-based spectral-amplitude-coding optical CDMA systems,” *J. Lightw. Technol.*, vol. 19, no. 9, pp. 1274–1281, Sep. 2001.

[5] X. Wang, W. Shi, H. Yun, S. Grist, N. A. F. Jaeger, and L. Chrostowski, “Narrow-band waveguide Bragg gratings on SOI wafers with CMOS-compatible fabrication process,” *Opt. Express*, vol. 20, no. 14, pp. 15547–15558, Jun. 2012.

[6] H.-C. Kim, K. Ikeda, and Y. Fainman, “Tunable transmission resonant filter and modulator with vertical gratings,” *J. Lightw. Technol.*, vol. 25, no. 5, pp. 1147–1151, May 2007.

[7] Z. Zhang, D. Liu, D. de Felipe, A. Liu, N. Keil, and N. Grote, “Polymer embedded silicon nitride thermally tunable Bragg grating filters,” *Appl. Phys. Lett.*, vol. 102, no. 18, May 2013, Art. no. 181105.

[8] P. Cheben, D.-X. Xu, S. Janz, and A. Densmore, “Subwavelength waveguide grating for mode conversion and light coupling in integrated optics,” *Opt. Express*, vol. 14, no. 11, pp. 4695–4702, May 2006.

[9] M. Hochberg and T. Baehr-Jones, “Towards fabless silicon photonics,” *Nat. Photon.*, vol. 4, no. 8, pp. 492–494, Aug. 2010.

[10] X. Wang, W. Shi, R. Vafaei, N. A. F. Jaeger, and L. Chrostowski, “Uniform and sampled Bragg gratings in SOI strip waveguides with sidewall corrugations,” *IEEE Photon. Technol. Lett.*, vol. 23, no. 5, pp. 290–292, Mar. 2011.

[11] M. Spasojevic and L. R. Chen, “Discretely tunable optical delay lines using serial and step-chirped sidewall Bragg gratings in SOI,” *Electron. Lett.*, vol. 49, no. 9, pp. 608–610, Apr. 2013.

[12] X. Wang, W. Shi, S. Grist, H. Yun, N. A. F. Jaeger, and L. Chrostowski, “Narrow-band transmission filter using phase-shifted Bragg gratings in SOI waveguide,” in *Proc. IEEE Photon. Conf.*, Oct. 2011, pp. 869–870.

[13] W. Zhang, N. Ehteshami, W. Liu, and J. P. Yao, “Silicon-based on-chip electrically tunable sidewall-Bragg-grating Fabry–Perot filter,” *Opt. Lett.*, vol. 40, no. 13, pp. 3153–3156, Jul. 2015.

[14] M. Caverley, X. Wang, K. Murray, N. A. F. Jaeger, and L. Chrostowski, “Silicon-on-insulator modulators using a quarter-wave phase-shifted Bragg grating,” *IEEE Photon. Technol. Lett.*, vol. 27, no. 22, pp. 2331–2334, Nov. 2015.

[15] Z. Pan *et al.*, “Tunable chromatic dispersion compensation in 40 Gbit/s systems using nonlinearly chirped fiber Bragg grating,” *J. Lightw. Technol.*, vol. 20, no. 12, pp. 2239–2246, Dec. 2002.

[16] J. Lim, K. Lee, J. Kim, and B. Lee, “Tunable fiber gratings fabricated in photonic crystal fiber by use of mechanical pressure,” *Opt. Lett.*, vol. 29, no. 4, pp. 331–333, Feb. 2004.

[17] H. Shahoei and J. P. Yao, “Continuously tunable slow and fast light by using an optically pumped tilted fiber Bragg grating written in an erbium/ytterbium co-doped fiber,” *IEEE Photon. Technol. Lett.*, vol. 24, no. 10, pp. 818–820, May 2012.

[18] K. Bédard, A. D. Simard, B. Filion, Y. Painchaud, L. A. Rusch, and S. LaRochelle, “Dual phase-shift Bragg grating silicon photonic modulator operating up to 60 Gb/s,” *Opt. Express*, vol. 24, no. 3, pp. 2413–2419, Feb. 2016.

[19] W. Shi, V. Veerasubramanian, D. Patel, and D. V. Plant, “Tunable nanophotonic delay lines using linearly chirped contradirectional couplers with uniform Bragg gratings,” *Opt. Lett.*, vol. 39, no. 3, pp. 701–703, Feb. 2014.

[20] E. Sahin, K. J. Ooi, C. E. Png, and D. T. H. Tan, “Large, scalable dispersion engineering using cladding-modulated Bragg gratings on a silicon chip,” *Appl. Phys. Lett.*, vol. 110, no. 16, Apr. 2017, Art. no. 161113.

[21] X. Wang *et al.*, “A silicon photonic biosensor using phase-shifted Bragg gratings in slot waveguide,” *J. Biophoton.*, vol. 6, no. 10, pp. 821–828, Oct. 2013.

[22] Q. Fang *et al.*, “Carrier-induced silicon Bragg grating filters with a p-i-n junction,” *IEEE Photon. Technol. Lett.*, vol. 25, no. 9, pp. 810–812, May 2013.

[23] A. W. Fang, E. Lively, Y.-H. Kuo, D. Liang, and J. E. Bowers, “A distributed feedback silicon evanescent laser,” *Opt. Express*, vol. 16, no. 7, pp. 4413–4419, Mar. 2008.

[24] R. Christen, “Reconfigurable bandpass filter with a three-to-one switchable passband width,” *IEEE Trans. Microw. Theory Techn.*, vol. 51, no. 2, pp. 573–577, Feb. 2003.

[25] Z. Li, Y. Han, H. Chi, X. Zhang, and J. P. Yao, “A continuously tunable microwave fractional Hilbert transformer based on a nonuniformly-spaced photonic microwave delay-line filter,” *J. Lightw. Technol.*, vol. 30, no. 12, pp. 1948–1953, Jun. 2012.

[26] W. Zhang and J. P. Yao, “Fully reconfigurable silicon-based waveguide Bragg grating for integrated microwave photonic applications,” in *Proc. Opt. Fiber Commun. Conf. Expo.*, M1H.1, Mar. 2018.

[27] W. Zhang and J. P. Yao, “A fully reconfigurable waveguide Bragg grating for programmable photonic signal processing,” *Nature Commun.*, vol. 9, Apr. 2018, Art. no. 1396.

[28] C. Roeloffzen *et al.*, “Silicon nitride microwave photonic circuits,” *Opt. Express*, vol. 21, no. 19, pp. 22937–22961, Sep. 2013.

[29] Y. Dai, X. Chen, D. Jiang, S. Xie, and C. Fan, “Equivalent phase shift in a fiber Bragg grating achieved by changing the sampling period,” *IEEE Photon. Technol. Lett.*, vol. 16, no. 10, pp. 2284–2286, Oct. 2004.

[30] J. Li *et al.*, “Experimental demonstration of distributed feedback semiconductor lasers based on reconstruction-equivalent-chirp technology,” *Opt. Express*, vol. 17, no. 7, pp. 5240–5245, 2009.

[31] W. Li, X. Zhang, and J. P. Yao, “Experimental demonstration of a multi-wavelength distributed feedback semiconductor laser array with an equivalent chirped grating profile based on the equivalent chirp technology,” *Opt. Express*, vol. 21, no. 17, pp. 19966–119971, Aug. 2013.

[32] J. Sun, C. W. Holzwarth, and H. I Smith, “Phase-shift Bragg grating in silicon using equivalent phase-shift method,” *IEEE Photon. Technol. Lett.*, vol. 24, no. 1, pp. 25–27, Jan. 2012.

[33] J. Sun *et al.*, “Uniformly spaced λ/4-shifted Bragg grating array with wafer-scale CMOS-compatible process,” *Opt. Lett.*, vol. 38, no. 20, pp. 4002–4004, Oct. 2013.

[34] V. Jayaraman, Z. M. Chuang, and L. A. Coldren, “Theory, design, and performance of extended tuning range semiconductor lasers with sampled gratings,” *IEEE J. Quantum Electron.*, vol. 29, no. 6, pp. 1824–1834, Jun. 1993.

[35] D. Huang, P. Pintus, and J. Bowers, "Towards heterogeneous integration of optical isolators and circulators with lasers on silicon," *Opt. Mater. Express*, vol. 8, no. 9, pp. 2471–2483, Sep. 2018.

[36] X. Chen, Y. Luo, C. Fan, T. Wu, and S. Xie, "Analytical expression of sampled Bragg gratings with chirp in the sampling period and its application in dispersion management design in a WDM system," *IEEE Photon. Technol. Lett.*, vol. 12, no. 8, pp. 1013–1015, Aug. 2000.

[37] W. Zhang, W. Li, H. Shahoei, and J. P. Yao, "Independently tunable multichannel fractional-order temporal differentiator based on a silicon-photonic symmetric Mach–Zehnder interferometer incorporating cascaded microring resonators," *J. Lightw. Technol.*, vol. 33, no. 2, pp. 361–367, Jan. 2015.

[38] R. Cheng and L. Chrostowski, "Multichannel photonic Hilbert transformers based on complex modulated integrated Bragg gratings," *Opt. Lett.*, vol. 43, no. 5, pp. 1031–1034, Mar. 2018.

Weifeng Zhang (S'12–M'17) received the B.Eng. degree in electronic science and technology from Xi'an Jiaotong University, Xi'an, China, in 2008, and the M.A.Sc. and Ph.D. degrees in electrical engineering from the Politecnico di Torino, Torino, Italy, and the University of Ottawa, Ottawa, ON, Canada, in 2011 and 2017, respectively. He is currently a Postdoctoral Fellow with the Microwave Photonics Research Laboratory, School of Electrical Engineering and Computer Science, University of Ottawa. His current research interests include silicon photonics and its applications in microwave photonics.

Jianping Yao (M'99–SM'01–F'12) received the Ph.D. degree in electrical engineering from the Université de Toulon et du Var, Toulon, France, in December 1997.

He is a Distinguished University Professor and the University Research Chair with the School of Electrical Engineering and Computer Science, University of Ottawa, Ottawa, ON, Canada. From 1998 to 2001, he was with the School of Electrical and Electronic Engineering, Nanyang Technological University (NTU), Singapore, as an Assistant Professor. In December 2001, he was with the School of Electrical Engineering and Computer Science, University of Ottawa, as an Assistant Professor, where he was promoted to an Associate Professor in May 2003, and a Full Professor in May 2006. He was appointed as the University Research Chair in Microwave Photonics in 2007. In June 2016, he was conferred the title of a Distinguished University Professor with the University of Ottawa. From July 2007 to June 2010 and July 2013 to June 2016, he was the Director of the Ottawa-Carleton Institute for Electrical and Computer Engineering. He has authored or coauthored over 560 research papers including more than 330 papers in peer-reviewed journals and more than 230 papers in conference proceedings.

Prof. Yao is the Editor-in-Chief for the IEEE PHOTONICS TECHNOLOGY LETTERS, a Topical Editor for *Optics Letters*, an Associate Editor for *Science Bulletin*, a Steering Committee Member of the JOURNAL OF LIGHTWAVE TECHNOLOGY, and an Advisory Editorial Board member of *Optics Communications*. He was a Guest Editor of a Focus Issue on Microwave Photonics in *Optics Express* in 2013, a Lead-Editor of a Focus Issue on Microwave Photonics in *Photonics Research* in 2014, and a Guest Editor of a special issue on Microwave Photonics in the IEEE JOURNAL OF LIGHTWAVE TECHNOLOGY in 2018. He is currently the Chair of the IEEE Photonics Ottawa Chapter, and is the Technical Committee Chair of IEEE MTT-3 Microwave Photonics. He was a member of the European Research Council Consolidator Grant Panel in 2016, the Qualitative Evaluation Panel in 2017, and a member of the National Science Foundation Career Awards Panel in 2016. He was the Chair of a number of international conferences, symposia, and workshops, including the Vice Technical Program Committee (TPC) Chair of the 2007 IEEE Topical Meeting on Microwave Photonics, the TPC Co-chair of the 2009 and 2010 Asia-Pacific Microwave Photonics Conference, the TPC Chair of the high-speed and broadband wireless technologies subcommittee of the IEEE Radio Wireless Symposium 2009–2012, the TPC Chair of the microwave photonics subcommittee of the IEEE Photonics Society Annual Meeting 2009, the TPC Chair of the 2010 IEEE Topical Meeting on Microwave Photonics, the General Co-chair of the 2011 IEEE Topical Meeting on Microwave Photonics, the TPC Co-chair of the 2014 IEEE Topical Meetings on Microwave Photonics, and the General Co-chair of the 2015 and 2017 IEEE Topical Meeting on Microwave Photonics. He has also served as a committee member for a number of international conferences, such as IPC, OFC, BGPP, and MWP. He was the recipient of 2005 International Creative Research Award of the University of Ottawa, the 2007 George S. Glinski Award for Excellence in Research, the Natural Sciences and Engineering Research Council of Canada Discovery Accelerator Supplements Award in 2008, and an inaugural OSA Outstanding Reviewer Award in 2012. He was also the recipient of the Award for Excellence in Research 2017–2018 of the University of Ottawa. He was one of the top ten reviewers of JOURNAL OF LIGHTWAVE TECHNOLOGY for 2015–2016. He was the IEEE MTT-S Distinguished Microwave Lecturer for 2013–2015. He is a registered Professional Engineer of Ontario. He is a Fellow of the Optical Society of America, the Canadian Academy of Engineering, and the Royal Society of Canada.